Coke Formation and Its Effects on Shape Selective Adsorptive and Catalytic Properties of Ferrierite

Wen-Qing Xu,[†] Yuan-Gen Yin,[†] Steven L. Suib,*[,†,‡,§] and Chi-Lin O'Young*[,⊥]

U-60, Department of Chemistry, Department of Chemical Engineering, and Institute of Materials Science, University of Connecticut, Storrs, Connecticut 06269-3060; and Texaco, Inc., Research & Development, P.O. Box 509, Beacon, New York 12508

Received: July 8, 1994; In Final Form: October 25, 1994[⊗]

Channels or cavities of ferrierite are blocked by carbonaceous deposits (coke) which are formed during butene treatments. The pore blocking inside ferrierite/alumina catalysts affects the yield and selectivity to isobutylene in the catalytic reaction of butene isomerization. Pore size distribution experiments show that the blocking of 10-member ring channels (4.2 × 5.4 Å) and 8-member ring channels (3.5 × 4.8 Å) of ferrierite by coke reduces the channel size smaller than that of the nitrogen molecule (4.09 Å). TPD data show that ammonia uptake for coked samples of different times on stream is decreased from about 62% to 35% of that for the fresh sample. This suggests that channels in coked ferrierites are at least larger than the size of the ammonia molecule (2 Å). Uptakes for more bulky molecules such as 1-butene (2.99 × 4.71 Å) and isobutylene (3.28 × 4.14 Å) are severely reduced by coke formation (< 9% of 1-butene and isobutylene uptakes for the fresh sample). About 76.9% of the coke formed after 18 h is deposited inside the micropores (<10 Å) of ferrierite/alumina. Modification of pore shapes through such coke deposition favors reactions involving small molecules, such as butene isomerization to isobutylene. In addition, kinetics studies of coke formation with microbalance methods reveal that the amount of coke deposit is limited to less than 11.1 wt % by the micropore volume of ferrierite. Such coke is aromatic in nature, and its hydrogen to carbon ratio decreases with time on stream. Acid sites on ferrierite having different size constraints are classified as H^+(XL), H^+(L), and H^+(S) (XL = extra large, L = large, S = small) from a structural point of view. These three kinds of acid sites were successfully probed with ammonia, 1-butene, and isobutylene. These experiments suggest that the adsorption of probe molecules on ferrierite is also a shape selective process.

Introduction

Isomerization of butene to isobutylene is a commercially important process for the production of MTBE. Szabo et al.[1] and Choudhary[2] reported using fluorinated γ-alumina as a catalyst for this isomerization with limited success. Zeolites, as acid catalysts, might catalyze this isomerization if both acidity and pore size are suitable to achieve desirable activity and selectivity. If the pore size is too large, such as zeolite Y which has supercages of 13 Å in diameter with openings of 7.4 Å (12-member ring), coke formation in the large pore rapidly deactivates the zeolite catalysts (after several seconds).[3] ZSM-5, a medium-pore zeolite (5.3 × 5.6 Å, 5.1 × 5.5 Å), is a coke-resistant catalyst in the presence of olefins. For example, it is used as a catalyst for olefin interconversions.[4] However, the selectivity to isobutylene in butene isomerization for this zeolite is low partly because the strong acidity of ZSM-5 catalyzes side reactions, such as butene dimerization followed by cracking to light hydrocarbons. Substitution of aluminum with boron in ZSM-5 leads to a reduced acid strength, resulting in a suppression of dimerization and cracking and an improvement in the selectivity to isobutylene.[5−8] Further suppression of butene dimerization is limited for boron-substituted ZSM-5 due to its medium-size pore.[6−8] In order for butene to dimerize inside the zeolite pore, the pore size has to be large enough to accommodate the products of the dimerization. For ZSM-5, the pore size is large enough to accommodate octenes so that the pore size of ZSM-5 cannot prohibit the dimerization.

Therefore, small pore zeolites such as ferrierite,[9] ZSM-23,[10] and ZSM-22[11] then came to our attention. For example, Texaco Inc. has recently patented in the United States of America that ferrierite, a small-pore zeolite as compared to ZSM-5, is a good catalyst for butene isomerization.[12] Shell and Lyondell oil companies have also patented the same process in Europe.[13,14] It is also reported that Lyondell is on the way to commercialize this process in Texas, United States of America.[15]

Ferrierite has been successfully synthesized by several methods. The organic templates involved in the preparation of ferrierite are alkene−polyamines,[16] 1,4-diaminocyclohexane,[17] cholin,[18] piperidine,[19] pyrrolidine,[20,21] and cyclohexylamine.[22] Silicon-to-aluminum ratios for synthetic ferrierite have been reported to range from 5 to 30. Aluminum-free ferrierite has also been prepared from aqueous silica solutions containing boric acid with ethylenediamine as the structure director or template.[23] Without any organic template, ferrierite can only be synthesized under stirring conditions. The resulting product has a narrow range of silicon-to-aluminum ratios centered approximately at nine.[24]

Vaughan[25] has shown that ferrierite has an orthorhombic framework containing one-dimensional channels of 10-member rings (4.2 × 5.4 Å) and one-dimensional channels of 8-member rings (3.5 × 4.8 Å). These two kinds of channels are perpendicularly intersected. The 8-member ring channels contain spherical cavities with a size of about 6−7 Å. In addition, 6- and 5-member rings are necessary to construct the framework of ferrierite.

Ferrierite with such a unique pore structure has distinctive adsorptive and catalytic properties. It shows exceptionally high

* To whom correspondence should be addressed.
† Department of Chemistry, UC.
‡ Department of Chemical Engineering, UC.
§ Institute of Materials Science, UC.
⊥ Texaco, Inc.
⊗ Abstract published in *Advance ACS Abstracts*, December 1, 1994.

0022-3654/95/2099-0758$09.00/0

para-selectivity in ethylbenzene disproportionation.[26] It is also a good catalyst for the isomerization of *o*- or *m*-xylene to *p*-xylene.[26,27] However, such pore structure leads to rapid coke formation and deactivation[26] for reactions involving aromatics. Normal alkane cracking[28-31] and methanol conversion[30-34] have been extensively studied on synthetic ferrierites. Hydrothermal treatment of ferrierites leads to extraction of aluminum from the framework and to a decrease in catalytic activity.[31,32] However, the aluminum extracted from the framework remains within the pores or channels even after the steamed ferrierites are leached with hydrochloric acid.[31]

In this study, butene isomerization over ferrierite has been investigated. The adsorption of ammonia, 1-butene, and isobutylene on ferrierite was studied in order to elucidate shape selectivity characteristics of the catalyst. In addition, we studied the process of coke formation, especially the location and the hydrogen-to-carbon ratio of the coke, in order to understand the critical role of coke in determining selectivity and activity of the catalyst.

Experimental Section

Preparation of Catalysts. The mixed forms of sodium and potassium ferrierite and ferrierite/alumina were provided by TOSOH, U.S.A. (sample numbers: HSZ-720KOA and HSZ-720KOD, respectively). The ratio of SiO_2 to Al_2O_3 for ferrierite is 17.6. Ferrierite/alumina contains 75 wt % of ferrierite and 25 wt % of alumina. H−ferrierite/alumina and H−ferrierite were obtained by ion exchange of their alkali forms two times with 1 M aqueous solution of ammonium nitrate followed by 2 h calcination at 823 K in air. These ferrierite materials contain sodium and potassium ions of less than 0.05 wt %. In addition, samples C-2, C-11, and C-18 are the coked ferrierite/alumina materials which were collected in *n*-butene skeletal isomerization reactions after 2, 11, and 18 h, respectively.

Characterizations. Pore size distributions were determined by nitrogen adsorption and desorption data acquired on an Omicron Omnisorp 100CX adsorptive and desorptive apparatus. The Kelvin theory was used to determine the distributions of meso- and macropores. The Horvath−Kawazoe method[35] was used to determine the distribution of micropores.

Fourier transform infrared (FTIR) experiments were done on a Mattson GALAXY II spectrometer at a resolution of 4 cm^{-1} by using either KBr pellets or self-supporting wafers (10 mg). Pyridine chemisorption experiments were done on self-supported wafers in an *in situ* IR cell. The sample was dehydrated at 773 K for 5 h under a vacuum of 10^{-5} Torr followed by adsorption of purified pyridine vapor at room temperature for 15 min. Then the system was evacuated at 423 K overnight to remove physisorbed pyridine, and an infrared spectrum was then recorded.

Temperature-programmed desorption (TPD) experiments were done on a TPD apparatus described previously.[6,36] The sample was first heated from room temperature to 823 K at a ramping rate of 15 K/min and then soaked at 823 K for 1 h under a flow of 30 mL/min ultrapure helium. The system was then cooled to 373 K over 100 min. Adsorbates (ammonia, 1-butene, or isobutylene) were then flowed over the sample for 30 min. The sample was then purged with helium for 40 min in order to eliminate physisorbed species. The temperature was ramped at 15 K/min from 373 to 883 K, and TPD data were acquired.

Catalysis. Butene isomerization reactions were run in a microreactor loaded with 140 mg of ferrierite/alumina at a pressure of 1 atm. The reactor was heated from room temperature to 823 K at a ramping rate of 15 K/min in a flow of nitrogen of 60 mL/min. The reactor was maintained at 823 K for 30 min. Then the reactor temperature was cooled to 693 K for 20 min. The reactor was then maintained at 693 K, and the nitrogen flow was switched to a mixture of 1-butene and nitrogen (1:1 molar ratio) at a space velocity of 8 whsv. The reaction products were analyzed every hour with a Hewlett-Packard 5890 Series II GC which was equipped with a GS-Alumina capillary column (J&W Scientific) and a thermal conductivity detector (TCD). The literature values for TCD response coefficients were used.[37,38]

The amounts and ratios of hydrogen to carbon of coke formed on ferrierite/alumina during butene isomerization were determined by coke combustion studies as described below. The coke combustion was carried out stepwise at 573, 673, 723, 773, 823, and 873 K under a flow of oxygen in a microreactor loaded with 10 mg of coked sample. Carbon dioxide and water formed during coke combustion were collected downstream in a cold trap (113.5 K) which consisted of isopentane and liquid nitrogen. Another cold trap of isopentane/liquid nitrogen was used upstream of the reactor to trap the moisture from the oxygen source. The moisture from the sample itself was subtracted by determining this amount from a similar experiment except using helium instead of using an oxygen flow. After 15 min of reaction all trapped products were evaporated and flushed into a TCD detector in an Varian 1400 Series GC. Water and carbon dioxide were separated because carbon dioxide evaporates onto the TCD first and has a short retention time. The amount and the ratio of hydrogen to carbon of coke are deduced from the amounts of water and carbon dioxide formed during combustion. The carbon dioxide peak was calibrated with a 34.4 μmol sample loop. TCD response coefficients for water and carbon dioxide[37] were used together to calibrate the water peak.

Experiments on the kinetics of coke formation were conducted on a custom-built system equipped with a Cahn 2000 microbalance and metallic enclosure under static conditions. The volume of the system is about 3.6 L. The detection limit for this balance is 5×10^{-6} g. About 25−35 mg of steamed or unsteamed fresh ferrierite samples was placed on a sample holder. Then the temperature of the sample holder was heated stepwise from room temperature, 323, 373, 423, 473, 523, 573, 623, and 673 to 693 K at 10^{-5} Torr. Each step was maintained for 1 h, and then the temperature was raised again to the next step until the final temperature was reached. After the temperature of the sample holder was maintained at 693 K for more than 1 h, 1-butene was rapidly introduced into the system until the system pressure reached 380 Torr. Coke formation was monitored by weight gain of this sample.

Structural Modeling. Molecular sizes of ammonia, 1-butene, and isobutylene were computed, and the structure of ferrierite was modeled with INSIGHT II and DISCOVER software from BIOSYM.

Results

Butene Isomerization on Ferrierite/Alumina. Product distributions of butene isomerization over ferrierite/alumina at 693 K under a flow of a mixture of 1-butene and nitrogen were determined by GC analyses. The conversions, selectivities, and yields are plotted versus time on stream, as shown in Figure 1. Under reaction conditions, the isomerization of 1-butene to 2-butenes rapidly reaches equilibrium via double-bond migration. For calculation of conversion, the three isomers of *n*-butene are grouped together. Figure 1 shows that the conversion of *n*-butene decreases, and the yield and selectivity to isobutylene increase with time on stream. The byproducts

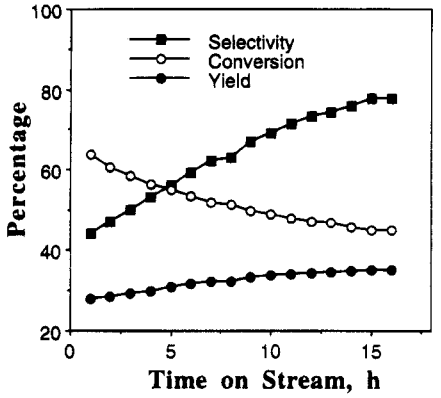

Figure 1. Conversion, selectivity to isobutylene, and yield of isobutylene for butene isomerization on ferrierite/alumina at 693 K.

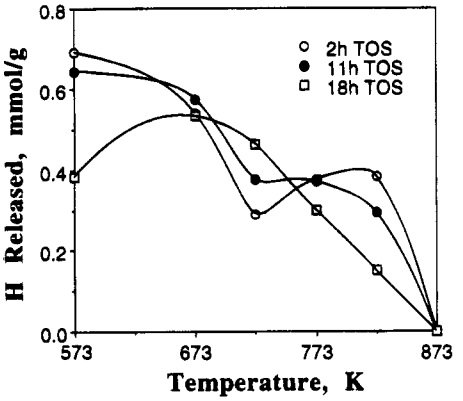

Figure 2. Amount of hydrogen released during coke combustion at different temperatures for coke deposited on ferrierite/alumina catalysts at different times on stream.

consist mainly of C2 to C8 olefins due to dimerization of *n*-butene followed by cracking. However, at the beginning of the reaction (<10 min), about 10% of the products consist of ethane, propane, and butanes. After 1 h, the amount of light alkanes in the products reduces to less than 2%.

Coke Combustion. Figure 2 shows the amount of hydrogen released during coke combustion at different temperatures for various coked catalysts for different times on stream. For the coked sample C-2, the amount of hydrogen released during combustion decreases with an increase of combustion temperature up to 723 K. Further increase of combustion temperature produces a peak that represents the amount of hydrogen released during combustion. It seems that there are two peaks for the amount of hydrogen released during coke combustion. When time on stream is increased to 11 h (sample C-11), these two peaks for the amount of hydrogen released during combustion are readily distinguished. In contrast, only one peak is observed for the amount of hydrogen released during combustion for the sample C-18. Figure 3 shows the amount of carbon dioxide released during coke combustion at different temperatures for various coked catalysts. When the combustion temperature is increased, C-2, C-11, and C-18 all show a maximum for the amount of carbon dioxide released. Furthermore, for the sample of longer time on stream (C-18), more carbon dioxide is released during combustion, and such increased amounts of carbon dioxide mainly fall in a range of temperature from 673 to 823 K.

Table 1 presents combustion data and summarizes total compositions of different cokes. The total amount of hydrogen decreases from 2.28 to 1.82 mmol/g, and the total amount of carbon increases from 2.46 to 3.84 mmol/g with increasing time on stream from 2 to 18 h. Accordingly, the ratio of hydrogen

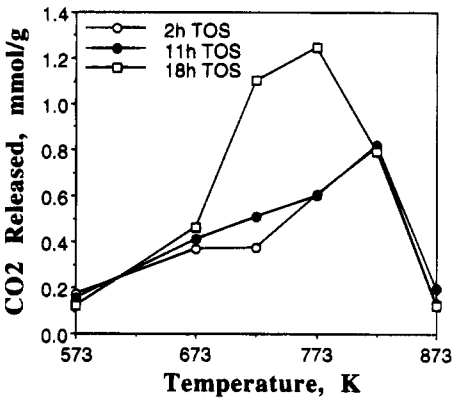

Figure 3. Amount of carbon dioxide released during coke combustion at different temperatures for coke deposited on ferrierite/alumina catalysts at different times on stream.

TABLE 1: Amounts of Hydrogen and Carbon Released during Coke Combustion at Different Temperatures for Used Ferrierite/Alumina Catalysts at Different Times on Stream

	2 h			11 h			18 h		
T, K	H[a]	C[a]	H/C	H[a]	C[a]	H/C	H[a]	C[a]	H/C
573	0.69	0.17	4.00	0.64	0.16	4.16	0.38	0.12	3.20
673	0.54	0.37	1.47	0.58	0.41	1.41	0.53	0.46	1.16
723	0.29	0.37	0.78	0.38	0.51	0.74	0.46	1.10	0.42
773	0.38	0.61	0.62	0.37	0.60	0.62	0.30	1.25	0.24
823	0.38	0.81	0.35	0.29	0.82	0.36	0.15	0.79	0.19
873	0.00	0.13	0.00	0.00	0.20	0.00	0.00	0.12	0.00
total[b]	2.28	2.46	0.93	2.26	2.70	0.84	1.82	3.84	0.47

[a] Unit is mmol/g. [b] Total composition of the coke.

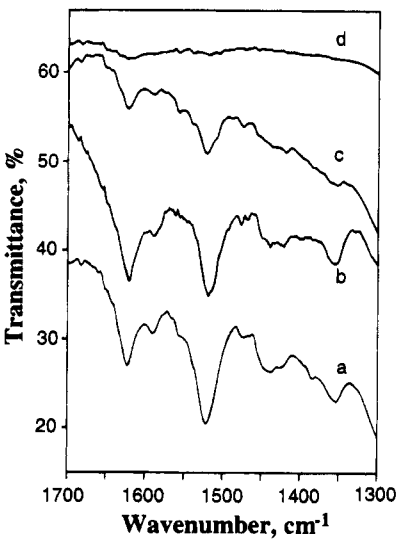

Figure 4. Infrared spectra of coke deposited on ferrierite/alumina catalysts at different times on stream: (a) C-2, (b) C-11, (c) C-18, (d) sample C-11 heated at 873 K in helium.

to carbon decreases with time on stream from 0.93 for the sample C-2 to 0.47 for the sample C-18. Table 1 also shows that the ratios of hydrogen to carbon which are released during coke combustion decrease from as high as 4.16 at 573 K to as low as 0.00 at 873 K.

Infrared Spectroscopy of Formed Cokes and Chemisorbed Pyridine on Ferrierite/Alumina. Infrared spectra of various coke deposits on ferrierite/alumina at different times on stream are shown in Figure 4. There are infrared bands at 1622, 1589, 1520, 1471, 1437, and 1352 cm^{-1} for all three coked samples (Figure 4, a, b, and c for C-2, C-11, and C-18, respectively). The intensities of these bands decrease with an increase in time

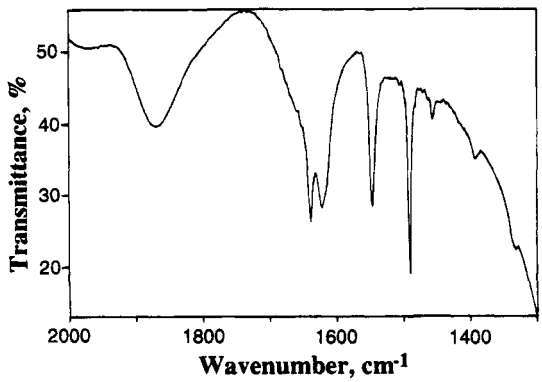

Figure 5. Infrared spectrum of pyridine adsorbed on ferrierite/alumina catalysts.

TABLE 2: Pore Size Distributions of the Fresh and Used H−Ferrierite/Alumina Catalysts

	pore volume (μL/g)	
pore radius (Å)	fresh	18 h
300−200	25	27
200−100	45	44
100−50	75	61
50−40	26	20
40−30	21	18
30−20	16	13
20−10	10	5.7
meso-, Macropore (>10 Å)	218	189
micropore (<10 Å)	96	0.8
surface area (total), m^2/g	316	52
surface area (>10 Å), m^2/g	88	51

on stream. After the sample C-11 was heated at 873 K in helium, properties of this coke were changed and this is evidenced by disappearance of all bands in the IR spectrum (Figure 4d).

Figure 5 shows pyridine adsorbed on the fresh ferrierite/alumina catalyst. There are infrared absorption bands at 1637, 1620, 1545, 1489, 1456, 1390, and 1330 cm^{-1}. Among these IR absorption bands, 1456 and 1545 cm^{-1} are due to pyridine molecules adsorbed on Lewis and Brønsted acid sites, respectively. The ratio of the peak area at 1545 cm^{-1} to that at 1456 cm^{-1} is 4.6.

Pore Size Distribution. Pore size distributions for fresh ferrierite/alumina and used ferrierite/alumina C-18 are listed in Table 2. For the fresh catalyst, there are 96 μL/g of micropore volume and 218 μL/g of meso- and macropore volume. After 18 h, the pore volume between 200 and 300 Å was slightly increased as compared to the fresh catalyst (from 25 to 27 μL/g). However, pores ranging from 10 to 300 Å were partially blocked (from 218 to 189 μL/g). Most of the micropores (smaller than 10 Å) were blocked by coke deposition (from 96 to 0.80 μL/g) during butene isomerization reactions.

Nitrogen molecules have a Pauling length of 4.09 Å, which is determined by $2^{1/6}\sigma$ (σ is a constant in the Lennard-Jones potential, 3.74 Å for nitrogen).[39] Therefore, nitrogen molecules are very difficult to enter the 8-member ring pores of ferrierite (3.5 × 4.8 Å). Theoretically, the micropore volume of ferrierite is estimated to be 150 μL/g by subtraction of the TO_2 volume (415 μL/g) from the framework volume (565 μL/g).

For zeolite systems, Breck[39] has assigned a value of 0.95 g/mL to the density of nitrogen instead of 0.808 g/mL (the density of liquid nitrogen). Therefore, the micropore volume of ferrierite determined by nitrogen adsorption is 109 μL/g, for example, (96 μL/g)(1/75%)[(0.808 g/mL)/(0.95 g/mL)]. Comparison of micropore volume data for ferrierite for experimental

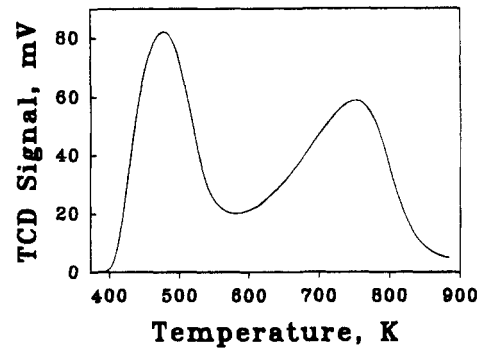

Figure 6. Ammonia TPD for the fresh ferrierite.

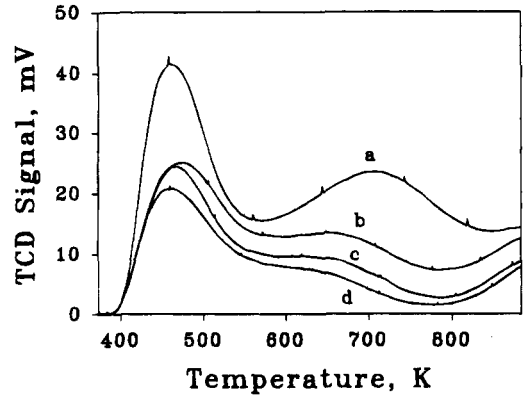

Figure 7. Ammonia TPD of fresh and used ferrierite/alumina catalysts: (a) fresh, (b) C-2, (c) C-11, and (d) C-18.

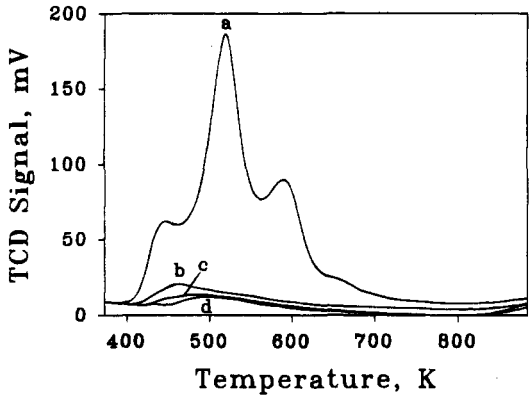

Figure 8. 1-Butene TPD of fresh and used ferrierite/alumina: (a) fresh, (b) C-2, (c) C-11, and (d) C-18.

(109 μL/g) and theoretical (150 μL/g) values suggests that nitrogen molecules do not enter the cavities of the 8-member rings in ferrierite.

Temperature-Programmed Desorption of Ammonia, 1-Butene, and Isobutylene. Figure 6 presents ammonia TPD results for the fresh ferrierite−ZSM-35. There are two desorption peaks of ammonia at 477 and 750 K. The total amount of desorbed ammonia for this fresh ferrierite is 2.35 mmol/g of catalyst. The ratio of the amount of desorbed ammonia at 750 K to that at 477 K is about 1.2.

Figure 7 shows ammonia TPD results for coked catalysts after different times on stream. The fresh catalyst of ferrierite/alumina shows two ammonia desorption peaks at 464 and 731 K, as shown in Figure 7a. As time on stream increases, the amount of acid sites decreases, as shown in Figure 7, b, c, and d for C-2, C-11, and C-18, respectively.

Figure 8 shows 1-butene TPD results for coked catalysts after different times on stream. The fresh catalyst (Figure 8a) has three desorption peaks at 445, 518, and 588 K and a shoulder

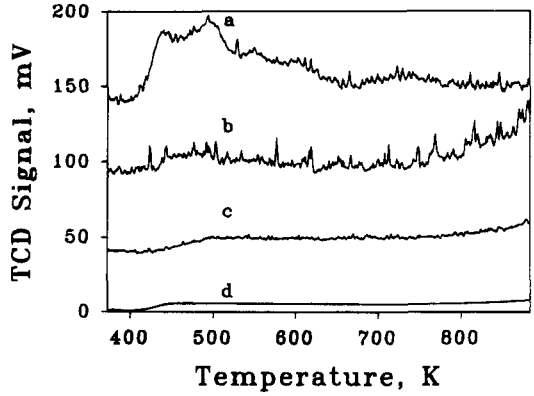

Figure 9. Isobutylene TPD of fresh and used ferrierite/alumina catalysts: (a) fresh, (b) C-2, (c) C-11, and (d) C-18.

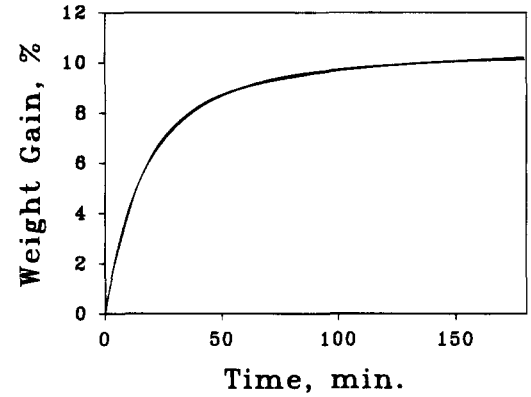

Figure 10. Weight gains for the fresh ferrierite in 1-butene at 380 Torr and 693 K.

at about 650 K. After this fresh catalyst was tested for butene isomerization for 2 h (C-2), the uptake of 1-butene decreases dramatically. The desorption peaks at 518, 588, and 650 K disappear. Only a small peak around 445 K is shown and shifted to higher temperature in Figure 8b. After increasing time on stream to 11 and 18 h (C-11 and C-18), no significant change was observed for the uptake of 1-butene (Figure 8c,d).

For isobutylene TPD experiments, there was a severe problem with dimerization of isobutylene to 2,4,4-trimethyl-1-pentene and 2,4,4-trimethyl-2-pentene when introducing isobutylene into the sample for adsorption at 373 K. The selectivity to the former product is as high as 94.5%. Significant amounts of liquid were observed to be condensed at the exit of the reactor during the adsorption process. Therefore, dimerization of isobutylene is an interference for the TPD data, and the resulting base line of the TPD data is very noisy. In any event, isobutylene TPD experiments yield some information about acid sites and pore shapes of the catalysts. Figure 9 shows isobutylene TPD data for coked catalysts after different times on stream. For the fresh catalyst (Figure 9a), there are basically two broad desorption peaks around 440 and 493 K. When time on stream is 2 h (C-2), the intensity of desorption is decreased as compared to the fresh catalyst (Figure 9a) but the base line is still noisy (Figure 9b). Coked catalyst C-11 (after 11 h) shows less desorption of hydrocarbons and the TPD base line becomes more smooth (Figure 9c). There is little isobutylene desorption observed in the isobutylene TPD for the coked catalyst C-18, and its base line is very smooth (Figure 9d).

Studies of Coke Formation Kinetics by Microbalance. Kinetic experiments of coke formation were conducted at static conditions in order to avoid disturbance of the microbalance as a result of flowing gas. After the fresh ferrierite was dehydrated at 693 K at a vacuum of 10^{-5} Torr, 1-butene at 380 Torr was introduced into the system. Then the weight gain was recorded. Coke formation at static conditions may be different from that at flowing conditions. Nevertheless, the studies of coke formation at static conditions will provide useful information. Figure 10 shows coke formation for the fresh ferrierite catalyst as a function of time. In general, coke formation on this catalyst is initially fast and then slowly decreases with time after introducing 1-butene into the system.

Discussion

Butene Isomerization and Coke Formation. Strong acidity of a zeolite leads to severe dimerization of olefins, and the majority of these dimers crack on such strong acid sites. Strong acid sites also result in rapid coke formation which may be an important factor responsible for the deactivation of zeolites in olefin processes. Large pores of zeolites also favor coke formation. For example, zeolite Y with a faujasite structure has very strong acidity as well as pores of large size (13 Å). Therefore, zeolite Y is not a good catalyst for *n*-butene isomerization. ZSM-5 also has very strong acidity which leads to interconversion of olefins.[4] The medium size pores of ZSM-5 limit coke formation to a certain degree. This may be the reason why ZSM-5 zeolites are now widely used as shape selective and coke resistant catalysts, such as for xylene isomerization, toluene disproportionation, conversion of methanol to gasoline, conversion of methanol to olefins, *etc.* But the medium pores of ZSM-5 are not outstanding for the selective isomerization of *n*-butenes to isobutylene.

Ferrierite is a small pore zeolite, and its acidity has been probed by pyridine chemisorption and ammonia TPD. IR spectra of ferrierite after pyridine chemisorption (Figure 5) show that ferrierite has both Brönsted and Lewis acid sites. The ratio of Brønsted to Lewis acid sites is about 6.2 to 6.4, which is estimated by multiplying the B/L area ratio (4.6) with average extinction coefficients (about 1.35−1.40).[40,41] A reviewer suggests that the amount of Brønsted acid sites is 165 μmol/g for this ferrierite sample, which is calculated from the absorbance of the IR band at 1540 cm^{-1}, based on Datka's method.[41,42] The amount of Brønsted acid sites (165 μmol/g) determined by pyridine chemisorption is about 10 times less than that (1.70 mmol/g) calculated from the aluminum content. Therefore, the reviewer suggests that pyridine molecules are too large to enter the micropores of ferrierite materials. Ammonia TPD (Figure 6) shows both strong acid sites (under desorption peak at 750 K) and weak acid sites (under desorption peak at 477 K). The ratio of the amount of strong acid sites to that of weak acid sites is 1.2.

After initially introducing 1-butene into ferrierite/alumina, coke deposition is very fast (as shown in Figure 10). Significant amounts of light alkanes were also observed due to hydrogen transfer to light olefins during formation of hydrogen deficient coke. As time on stream increases, the rate of coke deposition becomes slower and slower (Figure 10). In the meantime, formation of light alkanes becomes slower and slower. The yield and selectivity to isobutylene are increased with time on stream (Figure 1). This implies that, at early time on stream, olefins dimerize and are then cracked to lower olefins. Coke formation is mainly due to the high density of acid sites plus acid sites that have enough space around them for olefin dimerization and coke formation. As time on stream increases, some of these acid sites have been poisoned by coke that has been formed and some of the acid sites are blocked by such coke so that there is not enough space for the formation of olefin dimers. When dimerization of olefins and formation of coke

are suppressed, the yield and selectivity to isobutylene are improved.

Characteristics of the Deposited Coke. Coke deposited on ferrierite/alumina catalysts during butene isomerization to isobutylene has properties of aromatics. Infrared bands at 1622, 1589, 1520, 1471, 1437, and 1352 cm^{-1} in Figure 4 were observed for all cokes formed after different times on stream. Bands at 1622 cm^{-1} are assigned to C=C stretching vibrations of *n*-butenes.[43,44] The 1589 cm^{-1} band is due to microcrystalline polycyclic aromatics.[44] Coke with properties of aromatics also features an IR absorption band for aromatics (C=C stretching vibration) at 1520 cm^{-1}.[44] In addition, CH_3 and CH_2 groups attached to aromatics are also observed and evidenced by two IR bands at 1471 cm^{-1} (CH_2 deformation) and 1437 cm^{-1} (CH_3 asymmetric deformation).[43,44] While the amount of coke deposited on ferrierite/alumina increases with time on stream (as shown in Table 1 and Figure 10), the infrared band at 1520 cm^{-1} assigned to an aromatic structure is instead decreased with time on stream. This indicates, on one hand, that the coke grows from low polycyclic aromatics to high polycyclic aromatics with time on stream. Such a conclusion is also supported by the coke combustion experiments (Table 1); i.e., the ratio of hydrogen to carbon for cokes deposited on ferrierite/alumina decreases with time on stream.

Coke combustion experiments yield compositions of coke deposited on ferrierite/alumina (Table 1). The amount of hydrogen released during combustion decreases, and the amount of carbon released during combustion increases with time on stream for coked catalysts. Accordingly, the ratio of hydrogen to carbon decreases with time on stream for coke deposited on ferrierite/alumina. However, the ratios of hydrogen to carbon which are released during coke combustion for coked catalysts vary from as high as 4.16 for a combustion temperature of 573 K to as low as 0.00 for a combustion temperature of 873 K. It is difficult to understand why the coke deposits that are combusted at low temperature are like methane while coke combusted at high temperature is more like carbon. However, these phenomena imply that coke combustion is a complicated process in which hydrogen-rich coke is much more readily burned than carbon-rich coke. Complete burning of coke deposits from ferrierite/alumina requires a temperature as high as 873 K. In addition, the ratio of hydrogen to carbon and the amount of coke deposited on ferrierite/alumina vary with time on stream. The combustion process (Figure 2) shows that there is a two-step combustion for the coked sample C-2. When time on stream increases to 11 h (sample C-11), a two-step combustion process becomes less obvious. For the coked sample C-18, only a one-step combustion process was observed. Moreover, the increased coke deposit with time on stream mainly falls in a range of combustion temperatures from 673 to 823 K. These results further support IR data (discussed above) that suggest that the properties of coke change with time on stream.

Location of the Deposited Coke. Identification of the location of coke deposits is another approach for understanding the butene isomerization process. Coke formed after 18 h time on stream leads to partially blocked meso- or macropores (10–300 Å) from 218 to 189 μL/g (Table 2). However, such coke blocks most of the micropores (<10 Å) of ferrierite from 96 to 0.80 μL/g (Table 2). In other words, 76.9% of the coke forms in the micropores of ferrierite/alumina (such calculation is based on the volume of micropore blockage divided by the total volume of pore blockage). Moreover, micropore size distributions determined with the Horvath and Kawazoe method[35] are also shown in Figure 11. There is a sharp peak around 6 Å for fresh ferrierite/alumina (Figure 11a). After 18 h time on stream,

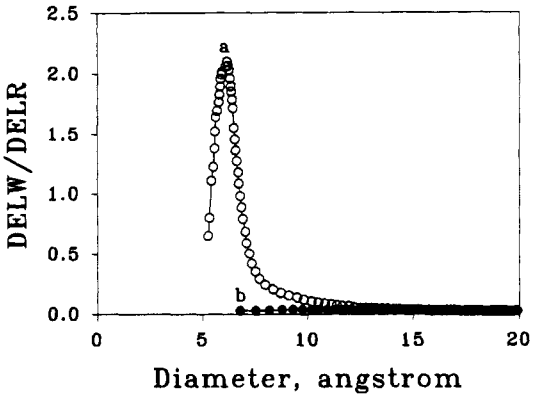

Figure 11. Micropore size distribution for fresh and used ferrierite/alumina catalysts: (a) fresh, (b) C-18.

TABLE 3: Percentage of Total Amount of Acidic Sites Available for Ammonia, 1-Butene, and Isobutylene on Ferrierite/Alumina Catalysts (4.44 [H^+]/Unit Cell)

sample	ammonia	1-butene	isobutylene[a]
fresh	100	74.1	30.8
2 h	62.1	8.8	6.6
11 h	47.7	4.7	4.2
18 h	35.1	4.2	3.0

[a] Amount of adsorbed isobutylene was roughly estimated due to noisy base lines in isobutylene TPD data (Figure 11).

the micropores of ferrierite/alumina are almost blocked, as shown in Figure 11b. From BET data, the micropores of the fresh ferrierite/alumina catalyst consist of 228 m^2/g of the total surface area (316 m^2/g, micro + meso + macro). The used catalyst C-18 only has 0.90 m^2/g micropore surface area with respect to a total surface area of 52 m^2/g.

Shape Selective Adsorption for Probing Different Acid Sites. The information obtained from using nitrogen as a probe to determine pore volumes, pore size distributions, and BET surface areas is limited. One reason is that nitrogen adsorption only gives information about physical properties of the catalysts. Ammonia TPD results (Figure 7) indicate that the number of both strong acid sites (ammonia desorption peak at high temperatures) and weak acid sites (ammonia desorption peak at low temperatures) are decreased by coke formation. At long time on stream, more acid sites are poisoned, or more acid sites are blocked off by the formed coke so as not to be accessible by ammonia. For 1-butene TPD (Figure 8) and isobutylene TPD (Figure 9) results, acid sites which are blocked by coke deposits from adsorption of 1-butene and isobutylene molecules are much greater as compared to ammonia molecules. Such blocking of adsorption of 1-butene or isobutylene on acid sites by coke is also enhanced with time on stream. Adsorption of 1-butene mainly occurs on weak acid sites since desorption peaks at high temperatures disappear for 1-butene TPD experiments of coked samples (Figure 8).

Quantitative data for ammonia, 1-butene, and isobutylene TPD studies are given in Table 3 (consider the uptake of ammonia as 100%). It is clearly shown that the larger the probe molecule, the more acid sites are blocked by coke deposits. It is assumed that one acid site adsorbs one probe molecule. The uptake of ammonia is considered as the total amount of acid sites existing in ferrierite/alumina catalysts.[6] For the fresh catalyst, only 74% of the acid sites are accessible for 1-butene adsorption and only 30% of the acid sites are accessible for isobutylene adsorption. These results further suggest that the accessibility of acid sites inside ferrierite/alumina depends on the size of the adsorbates. Acid sites located in certain positions of ferrierite may have space limitations for adsorption of large

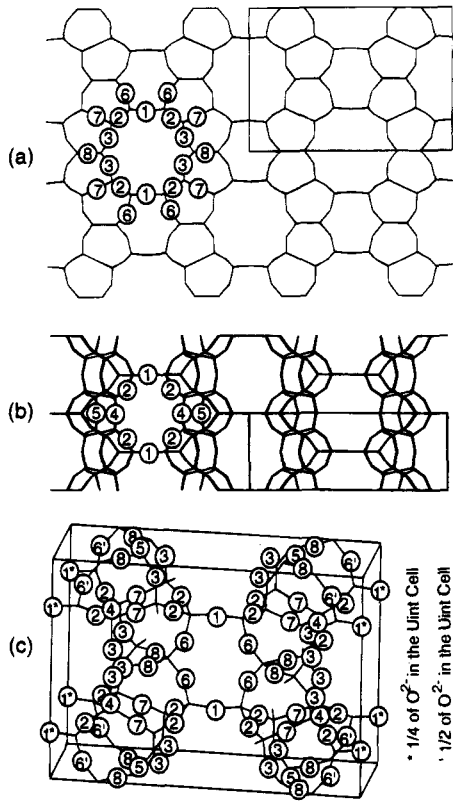

Figure 12. Ferrierite structure and location of eight kinds of O^{2-} ions: (a) [001] direction; (b) [010] direction; (c) a unit cell. Note: Arabic numbers in this figure are converted to Roman numerals in the text.

TABLE 4: Distribution of O^{2-} Ions in a Unit Cell of Ferrierite, $Si_{36}O_{72}$

type	I	II	III	IV	V	VI	VII	VIII
number	4	16	16	4	4	8	8	12

molecules such as 1-butene or isobutylene. Based on these data, the location of different sites which are responsible for adsorption of ammonia, 1-butene, and isobutylene molecules are of considerable interest.

Figure 12, a and b, shows the structure of ferrierite with views along the [001] and [010] directions, respectively. From the locations of O^{2-} ions in the ferrierite framework, O^{2-} ions can be classified among eight types, as specified in Figure 12a,b. Distribution of these eight types of O^{2-} ions is further specified in the unit cell of ferrierite (Figure 12c). Arabic numbers in Figure 12 are converted to Roman numerals for the convenience of discussion, and the number of O^{2-} ions for each type is tabulated in Table 4. The O^{2-} ions of type I, II, and IV are located in both 10-member and 8-member rings so that they have the largest space around them. These oxygen ions are grouped as O^{2-}(XL). The O^{2-} ions of type III and V are located inside the channels of the 10-member rings, and those of type VI are located inside the channels of the 8-member rings. Thus, symbol O^{2-}(L) is used to represent these O^{2-} ions of type III, V, and VI, which have large spaces around them. However, the O^{2-} ions of type VII and VIII are all located on 5-member rings so that the space around them is greatly limited and they are grouped as O^{2-}(S). The O^{2-}(XL) ions occupy 33.3% of all O^{2-} ions in the framework of ferrierite. The sum of O^{2-}(XL) and O^{2-}(L) ions represents 72.2% of all O^{2-} ions in the framework of ferrierite. It is assumed that the distribution of Al^{3+} ions inside ferrierite is random. One Al^{3+} leads to formation of one acid center which locates on the O^{2-} anion right next to this Al^{3+}. Therefore, acid sites located on O^{2-} ions can also be classified as H^+(XL), H^+(L), and H^+(S). From a statistical point of view, the percentage of H^+(XL), H^+(L), or H^+(S) is the same as that of the O^{2-}(XL), O^{2-}(L), or O^{2-}(S) ions, respectively. Interestingly, the percentage of H^+(XL), 33.3%, matches quite closely the amount of isobutylene adsorption, 30.8% (Table 3). The percentage of H^+(XL) and H^+(L), 72.2%, again matches quite closely the amount of 1-butene adsorption, 74.1% (Table 3). Such matches imply that the adsorption of these probe molecules is also shape selective. But-1-ene molecules can adsorb on all acid sites [H^+(XL) and H^+(L)] which are located in 10-member ring channels and in the 8-member ring cavities. Isobutylene molecules only adsorb on acid sites [H^+(XL)] which are located on both 10- and 8-member rings.

Our suggestion that but-1-ene molecules enter the 8-member ring cavities to access site VI is also supported by our adsorption data, as pointed out by a reviewer. The uptake of but-1-ene for fresh ferrierite in Table 3 (74% of 4.44/uc) can be converted to 85 μg/g of but-1-ene. The volume of adsorbed but-1-ene is 142 μL/g by using a but-1-ene density of 0.60 g/mL.[45] Therefore, the reviewer suggests that but-1-ene molecules enter the 8-member ring cavities by comparison of micropore volume data to theoretical (150 μL/g) data, to experimental data for nitrogen adsorption (109 μL/g), and to experimental data for but-1-ene adsorption (142 μL/g).

Kinetic Studies of Coke Formation. In this work, coke formation under static conditions was also studied with microbalance methods for the fresh ferrierite catalyst (Figure 10). The formation of coke on this sample is obviously related to the amount of acid sites. These microbalance data have been modeled with the following kinetic equation (eq 1):

$$dW/dt = k' P_{C_4H_8}{}^{\alpha}[H^+]^{\beta} \tag{1}$$

where W is the weight gain in g/100 g of cat., t the reaction time in min, $P_{C_4H_8}$ the pressure of 1-butene, [H^+] the amount of acid sites in mol/100 g of cat., α the reaction order of 1-butene, β the reaction order of acid sites, and k' the reaction constant. $P_{C_4H_8}$ is a constant (380 Torr), and therefore, $k'P_{C_4H_8}{}^{\alpha}$ is a constant and symbolized by k. The amount of acid sites ([H^+]) present on the catalyst decreases linearly with coke formation. Thus, acid sites occupied by the formed coke are expressed by the weight gain (W) times a constant (λ):

$$[H^+] = [H^+]_0 - \lambda W \tag{2}$$

where $[H^+]_0$ is the total amount of acid sites for a fresh catalyst.

Substituting eq 2 into eq 1 and integrating the resultant equation leads to eq 3 (based on an assumption that β is not equal to 1),

$$W = \frac{1}{\lambda} \frac{[H^+]_0\{[H^+]_0{}^{1-\beta} - k\lambda(1-\beta)t\}^{1/(\beta-1)} - 1}{\{[H^+]_0{}^{1-\beta} - k\lambda(1-\beta)t\}^{1/(\beta-1)}} \tag{3}$$

Coke formation data for the fresh ferrierite were fitted with eq 3. Resultant data from such fitting are plotted in Figure 10 along with experimental data and show that the proposed model is quite reasonable. The above assumption that β is not equal to 1 is met by the fitting result (β = 1.46). Other modeling parameters (λ and k) are equal to 2.27×10^{-2} and 5.00, respectively. Coke formation, W_∞, equals $[H^+]_0/\lambda$ when times approach infinity. Fresh ferrierite has $[H^+]_0$ of 0.235 mol/100 g of cat. Therefore, W_∞ is equal to 10.4 wt %. Our studies showed that other ferrierite samples which contain different amounts of acid sites ($[H^+]_0$) also have similar W_∞ (ranging

from 10.3 to 11.1 wt %). This suggests that the formation of coke is limited by the micropore volume of these ferrierite catalysts.

Conclusion

Yields and selectivities to isobutylene are increased with time on stream in skeletal isomerization of *n*-butene to isobutylene over ferrierite/alumina catalysts. At early time on stream, rapid coke formation is accompanied by formation of light alkanes in the products. These light alkanes originate from dimerization of butene with subsequent cracking and hydrogen transfer from coke formation. All these side reactions are mainly controlled by two factors, i.e., acidity and limitations of pore size. Coke deposition which increases with time on stream is controlled by the above two factors. Coke poisons acid sites to different extents depending on the acid strength. This leads to a suppression of dimerization reactions. Coke deposition also blocks channels and modifies the space around acid sites so that acid sites do not have enough space for dimerization reactions. Such blocking produces significant contributions for shape selectivity for skeletal isomerization of *n*-butene.

TPD results show that adsorption of ammonia, 1-butene, and isobutylene molecules is also shape selective. Bulky isobutylene molecules can only adsorb on acid sites of H^+(XL) which have the largest space around them. Small molecules of ammonia access all kinds of acid sites. Molecules of 1-butene can adsorb on acid sites of H^+(XL) extra large and H^+(L) large spaces. Any acid sites located on 5-member rings (H^+(S)) have too small a space around them for adsorption of any butene molecules. Moreover, coke formation on ferrierites shows considerable space limitations for adsorption of different large molecules. The larger the adsorbate molecule, the more blockage of the adsorbate from acid sites.

Modeling of coke formation data from microbalance studies suggests that the amount of coke formation is limited to less than 11 wt % by the micropore volume of ferrierite/alumina. The formation of coke is obviously related to the amount of acid sites. IR data for coke samples and results of coke combustion suggest that such coke is aromatic in nature and that the ratios of hydrogen to carbon increase with time on stream.

Acknowledgment. The authors thank Texaco Inc. and the Office of Basic Energy Sciences, Division of Chemical Sciences, Department of Energy, for their support of this research. The authors thank Mr. Xiao-Zhong Tang for his help in doing experiments of pore size distribution and BET measurements. We thank Dr. Suresh K. Gupta for his help in doing microbalance experiments. Mr. E. J. Neth and N.-G. Duan are also appreciated for computing molecular sizes of ammonia, 1-butene, and isobutylene and plotting structural graphs of ferrierite with INSIGHT II and DISCOVER software from BIOSYM.

References and Notes

(1) Szabo, J.; Perrotey, J.; Szabo, G.; Duchet, J. C.; Cornet, D. *J. Mol. Catal.* **1991**, *67*, 79–90.
(2) Choudhary, V. R. *Chem. Ind. Dev.* **1974**, *8*, 32.
(3) Wojciechowski, B. W.; Corma, A. *Catalytic Cracking: Catalysis, Chemistry and Kinetics*; Marcel Dekker: New York, 1986; p 100.
(4) Harandi, M. N.; Owen, O.; Mead, B. US Patent 5,024,679, June 18, 1991.
(5) Simon, M. W.; Nam, S. S.; Xu, W.-Q.; Suib, S. L.; Edwards, J. C.; O'Young, C.-L. *J. Phys. Chem.* **1992**, *96*, 6381–6388.
(6) Xu, W.-Q.; Suib, S. L.; O'Young, C.-L. *J. Catal.* **1993**, *144*, 285–295.
(7) Bianchi, D.; Simon, M. W.; Nam, S. S.; Xu, W.-Q.; Suib, S. L.; O'Young, C.-L. *J. Catal.* **1994**, *145*, 551–560.
(8) Simon, M. W.; Xu, W.-Q.; Suib, S. L.; O'Young, C.-L. *Microporous Mater.* **1994**, *2*, 477–486.
(9) Xu, W.-Q.; Yin, Y.-G.; Suib, S. L.; Edwards, J. C.; O'Young, C.-L. *J. Phys. Chem.*, submitted.
(10) Xu, W.-Q.; Yin, Y.-G.; Suib, S. L.; O'Young, C.-L. *J. Catal.* **1994**, *150*, 34–45.
(11) Simon, M. W.; Suib, S. L.; O'Young, C.-L. *J. Catal.* **1994**, *147*, 484–493.
(12) US Patent pending, assigned to Texaco, Inc.
(13) Grandvallet, P.; de Jong, K. P.; Mooiweer, H. H.; Kortbeek, A. G. T.; Kraushaar-Czarnetzki, B. European Patent 501,577, Feb 9, 1992.
(14) Powers, D. H.; Murray, B. D.; Winquist, B. H. C.; Callender, E. M.; Varner, J. H. European Patent 523,838, Jan 20, 1993.
(15) *C&E News* **1993** (Oct. 25), 30.
(16) Marosi, L.; Schwarzmann, M.; Stabenow, J. European Patent 49,-386, April 14, 1982.
(17) Hellring, S. D.; Chang, C. D.; Luther, J. D. US Patent 5,190,736, March 2, 1993.
(18) Plank, C. J.; Rosinski, E. J.; Rubin, M. K. US Patent 4,046,859, Sept 6, 1977.
(19) Nanne, J. M.; Post, M. F. M.; Stork, W. H. J. European Patent 12,473, June 25, 1980.
(20) Suzuki, K.; Kiyozumi, Y.; Shin, S.; Fujisawa, K.; Watanabe, H.; Saito, K.; Noguchi, K. *Zeolite* **1986**, *6*, 290–298.
(21) Dutta, P. K.; Rao, K. M.; Park, J. Y. *Langmuir* **1992**, *8*, 722–726.
(22) Whittam, T. V. European Patent 103,981, March 28, 1984.
(23) Gies, H.; Gunawardance, R. P. *Zeolites* **1987**, *7*, 442–445.
(24) Inaoka, W.; Kasahara, S.; Fukushima, T.; Igawa, K. In *Synthesis and Characterization of Zeolites*; Inui, T., Namba, S., Tatsumis, T., Eds.; *Stud. Surf. Sci. Catal.* **1991**, *60*, 37.
(25) Vaughan, P. A. *Acta Crystallogr.* **1966**, *21*, 983–990.
(26) Rane, S. J.; Satyanarayana, C. V. V.; Chakrabarty, D. K. *Appl. Catal.* **1991**, *69*, 177–186.
(27) Seddon, D. *J. Catal.* **1986**, *98*, 1.
(28) Harrison, I. D.; Leach, H. F.; Whan, D. A. *Zeolites* **1987**, *7*, 21–27.
(29) Komarov, V. S.; Malashevich, L. N.; Pis'mennaya, A. V. *Dokl. Akad. Nauk BSSR* **1981**, *4*, 332.
(30) Jin, Y. S.; Auroux, A.; Vedrine, J. C. *Appl. Catal.* **1988**, *37*, 1–19.
(31) Jin, Y. S.; Auroux, A.; Vedrine, J. C. *Appl. Catal.* **1988**, *37*, 21–33.
(32) Kibby, C. L.; Perrotta, A. J.; Massoth, F. E. *J. Catal.* **1974**, *35*, 256.
(33) Malashevich, L. N.; Pis'mennaya, A. V. *Vestsi Akad. Nauk BSSR, Ser. Khim. Nauk* **1984**, *6*, 57.
(34) Malashevich, L. N.; Pis'mennaya, A. V.; Komarov, V. S. *Vestsi Akad. Nauk BSSR, Ser. Khim. Nauk* **1987**, *3*, 23–27.
(35) Horvath, G.; Kawazoe, K. *J. Chem. Eng. Jpn.* **1983**, *15*, 470–475.
(36) Xu, W.-Q.; Suib, S. L. *J. Catal.* **1994**, *145*, 65–72.
(37) Messner, A. E.; Rosie, D. M.; Argabright, P. A. *Anal. Chem.* **1959**, *31*, 230–233.
(38) Rosie, D. M. *Anal. Chem.* **1957**, *29*, 1263–1264.
(39) Breck, D. W. *Zeolite Molecular Sieves*; Krieger Publishing: Malabar, FL, 1974; p 634.
(40) Emeis, C. A. *J. Catal.* **1993**, *141*, 347–354.
(41) Datka, J.; Turek, A. M.; Jehng, J. M.; Wachs, I. E. *J. Catal.* **1992**, *135*, 186–199.
(42) Datka, J. *J. Chem. Soc., Faraday Trans. 1* **1981**, *77*, 2877–2881.
(43) Barnes, A. J.; Howells, J. D. R. *J. Chem. Soc., Faraday Trans. 2* **1973**, *69*, 532.
(44) Ghosh, A. K.; Kydd, R. A. *J. Catal.* **1986**, *100*, 185–195.
(45) Weast, R. C.; Astle, M. J. *Handbook of Chemistry and Physics*; CRC Press: Boca Raton, FL, 1982–83; p C-193.

JP941731M